Modeling, Identification and Control, Vol. 28, No. 4, 2007, pp. 105–112

Experimental Validation of a Marine Propeller Thrust Estimation Scheme*

Luca Pivano [1] Øyvind N. Smogeli [2] Tor Arne Johansen [1] Thor Inge Fossen [1]

[1] *Department of Engineering Cybernetics, Norwegian University of Science and Technology, N-7491 Trondheim, Norway. E-mail:* {luca.pivano, tor.arne.johansen, thor.inge.fossen}@itk.ntnu.no

[2] *Department of Marine Technology, Norwegian University of Science and Technology, Trondheim, Norway. E-mail:* Oyvind.Smogeli@marinecyb.com

Abstract

A thrust estimation scheme for a marine propeller has been experimentally tested in waves and with a device that simulates the influence of a vessel hull. The scheme is formed by a nonlinear propeller torque observer and a mapping to generate the thrust from the observed torque. The mapping includes the estimation of the advance number. This is utilized to improve the performance when the propeller is lightly loaded. The advance speed is assumed to be unknown, and only measurements of shaft speed and motor torque have been used. Accurate results have been obtained in experimental tests.

Keywords: Propulsion, state estimation, nonlinear, observers.

1 Introduction

In the design of vessel control systems, such as Dynamic Positioning (DP), thruster assisted Position Mooring (PM) and autopilot systems, much effort has been put into the high-level control schemes. More recently, also the issue of local thruster dynamics and control has received more attention. For recent references, see for example Bachmayer et al. (2000), Blanke et al. (2000), Whitcomb and Yoerger (1999), Smogeli et al. (2005), Smogeli (2006) and references therein. The ability to design a good control system is mainly limited by two difficulties: to model the vessel's and the propeller's dynamics and to measure the environmental state. For example in severe weather conditions high thrust losses due to ventilation, in-and-out-of water effects and wave-induced water velocities are experienced. There are also losses of thrust due to the interaction between the vessel hull and the propeller. Recently, observers for monitoring the propeller performance have been developed and included in new control designs for electrically driven propellers, see Guibert et al. (2005) and Smogeli (2006).

All these considerations motivate the development of schemes to estimate the propeller thrust because, in general, its measurement is not available. The incorporation of the estimated thrust in a controller could improve the overall control performance. Moreover the performance monitoring will also be important for improving thrust allocation in different working conditions of the propeller, from normal to extreme environmental operating conditions.

The problem of the propeller thrust estimation has been treated in Zhinkin (1989) where full-scale experimental results were provided for positive shaft speed and vessel speed in steady-state conditions, in waves, and for slanted inflow. The estimation was based on the propeller torque measurement and on a linear relation between thrust and torque.

Thrust estimation has been also treated in Guibert et al. (2005), where the estimate was computed

*Published at the 7th Conference on Manoeuvring and Control of Marine Craft (MCMC2006), Lisbon, Portugal, September 20-22, 2006.

ISSN 1890–1328 **doi:10.4173/mic.2007.4.2**

from the propeller torque obtained with a Kalman filter where a linear shaft friction torque was considered. The relation between thrust and torque involved an axial flow velocity model and required the knowledge of the advance speed, very difficult to measure in real vessel. The scheme was also highly sensitive to hydrodynamic and mechanical modelling errors. The results were presented in a simulation.

In Pivano et al. (2006b) a thrust estimation scheme that works in the four-quadrant plane composed by the vessel speed and the propeller shaft speed was proposed. The scheme involved a nonlinear observer for the propeller torque and a piecewise linear mapping to generate the propeller thrust from the observed torque. Accurate results were presented in Pivano et al. (2006b) for open-water tests with the propeller deeply submerged. In this paper the scheme presented in Pivano et al. (2006b) is considered and experimentally tested under different conditions. The mapping to compute the thrust from the propeller torque has been improved in order to increase the accuracy when the propeller is lightly loaded. Differently from Guibert et al. (2005) the advance speed is assumed to be unknown. The scheme has been tested in waves to reproduce rough sea conditions and with a device that simulates the influence of a vessel hull. Results show that the estimation scheme provides good estimates in both conditions.

2 Propeller and shaft dynamics modeling

A block diagram that represents the system is shown in Figure 1.

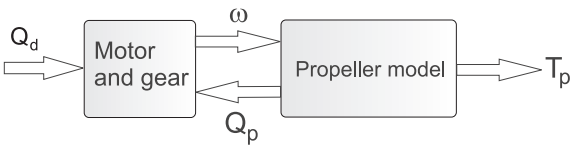

Figure 1: Propeller system block diagram.

The shaft dynamics is derived by considering an electric motor attached to a shaft influenced by friction. It can be written as:

$$J_m\dot{\omega} = Q_m - Q_p - Q_f(\omega), \tag{1}$$

where J_m is shaft moment of inertia and Q_f is the shaft friction torque which depends on the shaft speed. In this paper it will be considered as a Coulomb plus a linear and nonlinear viscous effect:

$$Q_f(\omega) = k_{f_1} \arctan\left(\frac{\omega}{\epsilon}\right) + k_{f_2}\omega + k_{f_3} \arctan(k_{f_4}\omega). \tag{2}$$

This is motivated by the experimental result of the system identification on the shaft friction torque for the propeller used for the experiments regarded in this paper (Pivano et al., 2006a). In order to avoid the discontinuity in zero, the Coulomb effect, usually written as a sign(ω), has been replaced by the function arctan($\frac{\omega}{\epsilon}$) with a small positive ϵ. All the coefficients k_{f_i} are constant and positive.

3 Thrust estimation scheme

The scheme implemented to derive the propeller thrust is shown in the block diagram of Figure 2. The propeller shaft speed ω and the motor torque Q_m are assumed to be measurable. First a stable observer is designed to estimate the propeller load torque Q_p. Second, an estimate of the propeller thrust T_p is computed from the estimated propeller torque.

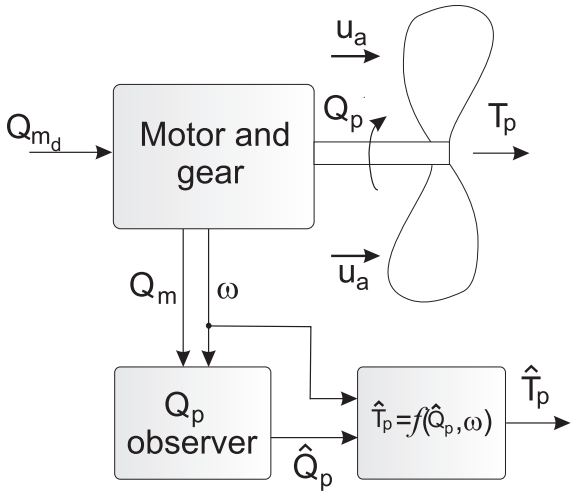

Figure 2: Propeller thrust estimation scheme.

3.1 Propeller torque observer

To derive a stable observer for the propeller torque the following system is considered (Pivano et al., 2006b):

$$J_m\dot{\omega} = Q_m - Q_p - Q_f(\omega) + \Delta_f, \tag{3}$$

$$\dot{Q}_p = -\frac{1}{\tau_q}Q_p + w_q, \tag{4}$$

where the propeller torque Q_p is treated as a time-varying parameter and modeled as a first order process

with positive time constant τ_q and driven by a bounded random noise w_q. In (3) a friction modeling error and measurement error on Q_m are accounted for by Δ_f. The following observer with gains L_1 and L_2 is proposed:

$$J_m\dot{\hat{\omega}} = Q_m - \hat{Q}_p - Q_f(\hat{\omega}) + L_1(y-\hat{y}), \tag{5}$$

$$\dot{\hat{Q}}_p = -\frac{1}{\tau_q}\hat{Q}_p + L_2(y-\hat{y}). \tag{6}$$

The measurement

$$y = \omega + v \tag{7}$$

is assumed to be corrupted by an error v. We assumed that Δ_f, v and w_q are bounded. With $\tilde{x}_1 = \omega - \hat{\omega} = x_1 - \hat{x}_1$ and $\tilde{x}_2 = Q_p - \hat{Q}_p = x_2 - \hat{x}_2$, the error dynamics can be written as:

$$\begin{aligned}\dot{\tilde{x}}_1 = {} & \frac{1}{J_m}\left[-\tilde{x}_2 - k_{f_1}\left(\arctan\left(\frac{x_1}{\epsilon}\right) - \arctan\left(\frac{\hat{x}_1}{\epsilon}\right)\right)\right] \\ & + \frac{1}{J_m}\left[-k_{f_3}\left(\arctan\left(k_{f_4}x_1\right) - \arctan\left(k_{f_4}\hat{x}_1\right)\right)\right] \\ & + \frac{1}{J_m}\left[-k_{f_2}\tilde{x}_1 - L_1\tilde{x}_1 + \Delta_f - L_1 v\right], \end{aligned} \tag{8}$$

$$\dot{\tilde{x}}_2 = -\frac{1}{\tau_q}\tilde{x}_2 - L_2\tilde{x}_1 - L_2 v + w_q. \tag{9}$$

Noise and measurement errors can be treated as inputs, grouped in the vector

$$u = \begin{bmatrix} u_1 & u_2 & u_3 \end{bmatrix} = \begin{bmatrix} \Delta_f & v & w_q \end{bmatrix}^T.$$

Proposition 3.1 *Suppose that the following assumptions are satisfied*

A1 $L_1 > -k_{f_2}$

A2 $\left|\frac{1}{J_m} + L_2\right| < 2\sqrt{\frac{1}{\tau_q}\left(\frac{k_{f_2}+L_1}{J_m}\right)}$.

Then the system of (8) and (9) is input-to-state stable (ISS) with respect u.

Proof Taking the Lyapunov function $V(\tilde{x}) := \frac{1}{2}\tilde{x}_1^2 + \frac{1}{2}\tilde{x}_2^2$, we can compute its time derivative along the trajectory of the system of (8) and (9):

$$\begin{aligned}\dot{V} = {} & -\frac{k_{f_2}}{J_m}\tilde{x}_1^2 - \frac{L_1}{J_m}\tilde{x}_1^2 - \frac{1}{\tau_q}\tilde{x}_2^2 - \frac{1}{J_m}\tilde{x}_2\tilde{x}_1 + \frac{1}{J_m}u_1\tilde{x}_1 \\ & -\frac{2}{\pi}\frac{k_{f_1}}{J_m}\left(\arctan\left(\frac{x_1}{\epsilon}\right) - \arctan\left(\frac{\hat{x}_1}{\epsilon}\right)\right)\tilde{x}_1 \\ & -\frac{k_{f_3}}{J_m}\left(\arctan\left(k_{f_4}x_1\right) - \arctan\left(k_{f_4}\hat{x}_1\right)\right)\tilde{x}_1 \\ & -\frac{L_1}{J_m}u_2\tilde{x}_1 - L_2\tilde{x}_1\tilde{x}_2 - L_2 u_2\tilde{x}_2 + u_3\tilde{x}_2. \end{aligned} \tag{10}$$

Since $\left[\arctan(a) - \arctan(b)\right](a-b) \geq 0$, we can rewrite (10) as:

$$\begin{aligned}\dot{V} \leq {} & -\frac{k_{f_2}}{J_m}\tilde{x}_1^2 - \frac{L_1}{J_m}\tilde{x}_1^2 - \frac{1}{\tau_q}\tilde{x}_2^2 + \frac{1}{J_m}u_1\tilde{x}_1 - \frac{L_1}{J_m}u_2\tilde{x}_1 \\ & -\frac{1}{J_m}\tilde{x}_2\tilde{x}_1 - L_2\tilde{x}_1\tilde{x}_2 - L_2 u_2\tilde{x}_2 + u_3\tilde{x}_2. \end{aligned} \tag{11}$$

If $u = 0$, (11) becomes:

$$\begin{aligned}\dot{V} & \leq -\frac{k_{f_2}}{J_m}\tilde{x}_1^2 - \frac{L_1}{J_m}\tilde{x}_1^2 - \frac{1}{\tau_q}\tilde{x}_2^2 - \frac{1}{J_m}\tilde{x}_2\tilde{x}_1 - L_2\tilde{x}_1\tilde{x}_2 \\ & \leq -\tilde{x}^T Q\tilde{x}, \end{aligned} \tag{12}$$

where $\tilde{x} = \begin{bmatrix}\tilde{x}_1 & \tilde{x}_2\end{bmatrix}^T$ and

$$Q = \begin{bmatrix} \frac{k_{f_2}+L_1}{J_m} & \frac{1}{2}\left(\frac{1}{J_m} + L_2\right) \\ \frac{1}{2}\left(\frac{1}{J_m} + L_2\right) & \frac{1}{\tau_q} \end{bmatrix} \tag{13}$$

If assumptions A1 and A2 hold, Q is positive definite and the origin of (8) and (9), with $u = 0$, is globally exponentially stable (GES), see Khalil (2000), since

$$\dot{V} \leq -\lambda_{\min}\{Q\}\left\|\tilde{x}\right\|_2^2 \leq 0,$$

where

$$\begin{aligned}\lambda_{\min}\{Q\} = {} & \frac{k_{f_2}+L_1}{2J_m} + \frac{1}{2\tau_q} \\ & -\frac{1}{2}\sqrt{\left(\frac{k_{f_2}+L_1}{J_m} + \frac{1}{\tau_q}\right)^2 + \left(\frac{1}{J_m} + L_2\right)^2 - 4\frac{k_{f_2}+L_1}{J_m\tau_q}} \end{aligned} \tag{14}$$

When $u \neq 0$, (11) can be written as follows:

$$\begin{aligned}\dot{V} \leq {} & -\lambda_{\min}\{Q\}\left\|\tilde{x}\right\|_2^2 + \frac{1}{J_m}\left\|u\right\|_\infty\left|\tilde{x}_1\right| \\ & + \frac{|L_1|}{J_m}\left\|u\right\|_\infty\left|\tilde{x}_1\right| + |L_2|\left\|u\right\|_\infty\left|\tilde{x}_2\right| + \left\|u\right\|_\infty\left|\tilde{x}_2\right| \\ \leq {} & -\lambda_{\min}\{Q\}\left\|\tilde{x}\right\|_2^2 \\ & + \left\|u\right\|_\infty\left[\left(\frac{1+|L_1|}{J_m}\right)\left|\tilde{x}_1\right| + \left(|L_2|+1\right)\left|\tilde{x}_2\right|\right] \end{aligned} \tag{15}$$

Using the following inequalities for $\tilde{x} \in R^2$: $\left\|\tilde{x}\right\|_\infty \leq \left\|\tilde{x}\right\|_2 \leq \sqrt{2}\left\|\tilde{x}\right\|_\infty$ and $a\left|\tilde{x}_1\right| + b\left|\tilde{x}_2\right| \leq \sqrt{a^2+b^2}\left\|\tilde{x}\right\|_2$,

it is possible to rewrite (15) as:

$$\begin{aligned}\dot{V} &\leq -\lambda_{\min}\{Q\}\,\|\tilde{x}\|_\infty^2 \\ &\quad + \|u\|_\infty \sqrt{\left(\frac{1+|L_1|}{J_m}\right)^2 + (|L_2|+1)^2}\sqrt{2}\,\|\tilde{x}\|_\infty \\ &\leq -(1-\theta)\lambda_{\min}\{Q\}\,\|\tilde{x}\|_\infty^2 - \theta\lambda_{\min}\{Q\}\,\|\tilde{x}\|_\infty^2 \quad (16) \\ &\quad + \|u\|_\infty \sqrt{2\left(\left(\frac{1+|L_1|}{J_m}\right)^2 + (|L_2|+1)^2\right)}\,\|\tilde{x}\|_\infty\end{aligned}$$

where $0 < \theta < 1$. For any $\|\tilde{x}\|_\infty$ such that

$$\|\tilde{x}\|_\infty \geq \frac{\|u\|_\infty \sqrt{2\left(\left(\frac{1+|L_1|}{J_m}\right)^2 + (|L_2|+1)^2\right)}}{\theta\lambda_{\min}\{Q\}} := \rho(\|u\|_\infty) \quad (17)$$

where $\rho(\cdot)$ is a class $\mathcal{K}$ function, we obtain:

$$\dot{V} \leq -(1-\theta)\lambda_{\min}\{Q\}\,\|\tilde{x}\|_\infty^2 \leq 0 \quad (18)$$

From Theorem 4.19 of Khalil (2000), the system of (8) and (9) is ISS. Furthermore, the observer error is uniformly ultimately bounded by $\rho\left(\sup_{t>t_0}(\|u\|_\infty)\right)$.

3.2 Thrust/torque relationship

The propeller thrust is closely related to the propeller torque and, in general, the relation is a nonlinear function. The results obtained from experimental test in Zhinkin (1989) showed that the relation between thrust and torque is very stable. This allows us to use the propeller torque, either measured or estimated, to compute the thrust when its measurement is not available. In Pivano et al. (2006b), it was shown that the relation between the propeller thrust and torque could be approximated with a linear piecewise function. The mapping showed good results on reproducing the thrust from the estimated propeller torque during various experimental tests. The linear relation between thrust and torque used in Pivano et al. (2006b) may not provide accurate results when the propeller is lightly loaded, i.e. working at high values of the advance number J. The advance number J is computed as:

$$J = \frac{2\pi u_a}{\omega D},$$

where D is the propeller disc diameter and u_a is the advance speed (the ambient inflow velocity of the water to the propeller). The advance speed is difficult to measure on real vessels and is normally different from the vessel speed due to the interaction between the vessel hull and the propeller. To relate the thrust and torque, the standard propeller characteristics K_T and K_Q are considered. From Van Lammeren et al. (1969) we have:

$$T_p = K_T \frac{\rho\omega^2 D^4}{4\pi^2}, \quad (19)$$

$$Q_p = \frac{K_Q \rho\omega^2 D^5}{4\pi^2}. \quad (20)$$

Figure 3 shows the measured propeller characteristics of the propeller considered in this paper.

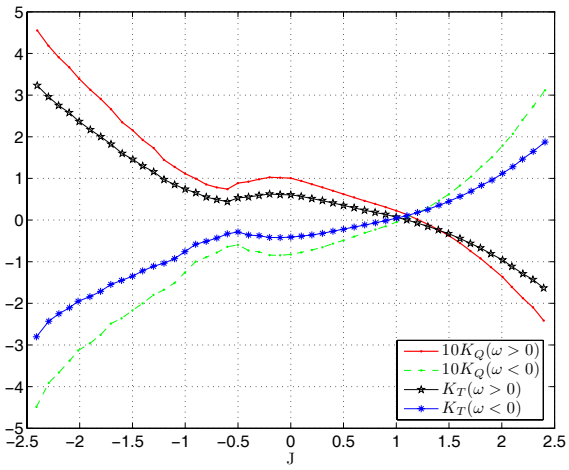

Figure 3: Propeller characteristics K_T and K_Q.

Figure 4 (b) shows the ratio between the propeller thrust and torque for positive shaft speed ω computed from the propeller characteristics of Figure 3 as:

$$\frac{T_p}{Q_p} = \frac{K_T}{K_Q D}. \quad (21)$$

In Figure 4 (b) we can see that for values of J greater than J_2, the thrust and torque ratio changes substantially and to compute accurately the thrust from the torque, the values of J need to be known. The procedure employed to estimate the thrust from the propeller torque is summarized in the following steps:

- Computation of $\hat{K}_Q$, an estimate of K_Q, solving (20) where $\hat{Q}_p$ is used instead of Q_p. From Figure 4 we can also see that for values of K_Q outside the region limited by K_Q^+ and K_Q^-, the ratio between thrust and torque is basically constant. For this reason the value of $\hat{K}_Q$ can be set to be equal to K_Q^+ when $\hat{K}_Q$ computed with (20) is greater than K_Q^+ and set to K_Q^- if $\hat{K}_Q$ is less than K_Q^-.
- Calculation of $\hat{J}$, an estimate of the advance number J, inverting the K_Q curve using the calculated $\hat{K}_Q$. From Figure 4 (a) we can see that it

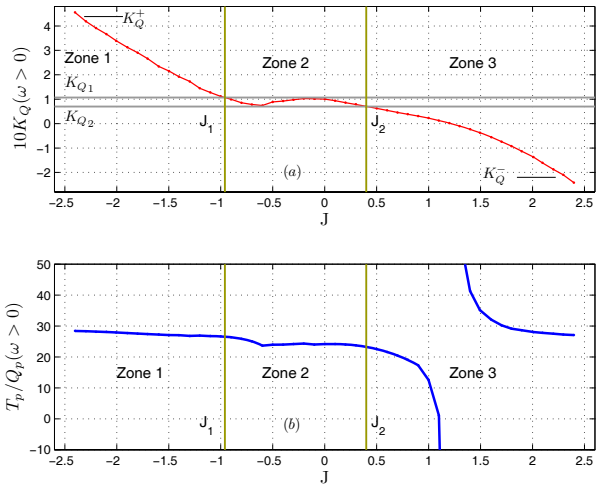

Figure 4: K_Q characteristic and the ratio between thrust and torque for $\omega > 0$.

is not possible to obtain exactly the value of J around zero because the K_Q curve in not invertible. To solve this problem the J axis has been divided in three zones as shown in Figure 4. In the zone 1 ($J < J_1$) and zone 3 ($J > J_2$) the K_Q curve is invertible and J can be find accurately. When $K_{Q_2} \leq K_Q \leq K_{Q_1}$(zone 2) we approximate $\hat{J}$ with zero. Since in zone 2 the ratio between thrust and torque does not change considerably, this approximation introduces a small error in the overall mapping.

- Computation of $\hat{K}_T$, an estimate of K_T, using the propeller characteristics and $\hat{J}$.
- Calculation of the thrust with (19) where $\hat{K}_T$ is used instead of K_T.

A block diagram that shows the procedure is presented in Figure 5.

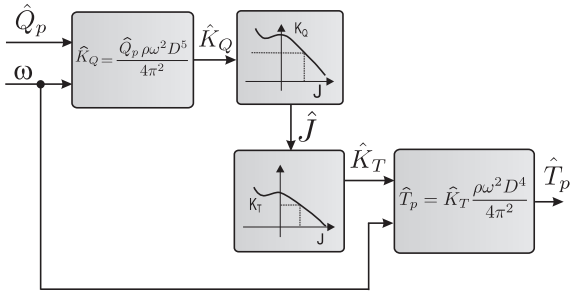

Figure 5: Thrust estimation block diagram.

4 Experimental results

4.1 Setup

The experiments were performed at the MCLab (www.itk.ntnu.no/marinkyb/MCLab/), an experimental laboratory located at NTNU (Trondheim, Norway). The basin, 6.45 m wide, 40 m long and 1.5 m deep, is equipped with a 6DOF towing carriage that can reach a maximum speed of 2 m/s and with a wave generator able to generate waves up to 0.3 m.

The tests have been performed on a four bladed propeller with a diameter of 0.25 m. A metallic grid has been placed upstream of the propeller in order to reduce the speed of the inflow to the propeller disc. In this way we could simulate the presence of the vessel hull. A sketch of the setup is shown in Figure 6.

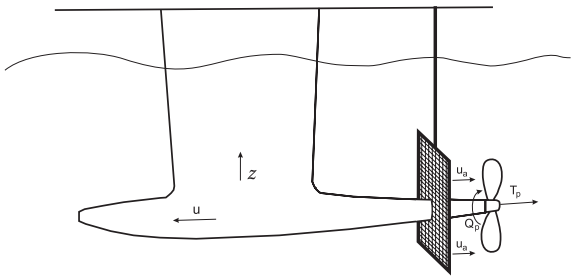

Figure 6: Sketch of the experimental setup.

Some tests were performed in order to measure the standard propeller characteristics shown in Figure 3 and to measure the four-quadrant propeller characteristics C_T and C_Q, plotted as a function of the advance angle β. The advance angle β is computed with the four-quadrant inverse tangent function as:

$$\beta = \arctan2\left(u_a, 0.7R\omega\right), \tag{22}$$

where R is the propeller disc radius. The four-quadrant thrust and torque coefficients are computed from Van Lammeren et al. (1969) as:

$$C_T = \frac{T_p}{\frac{1}{2}\rho V_r^2 A_0}, \tag{23}$$

$$C_Q = \frac{Q_p}{\frac{1}{2}\rho V_r^2 A_0 D}, \tag{24}$$

where A_0 is the propeller disc area, ρ is the water density, D is the propeller diameter and V_r is the relative advance velocity:

$$V_r^2 = u_a^2 + (0.7R\omega)^2. \tag{25}$$

The four-quadrant characteristics of to the propeller considered in this paper is shown in Figure 7.

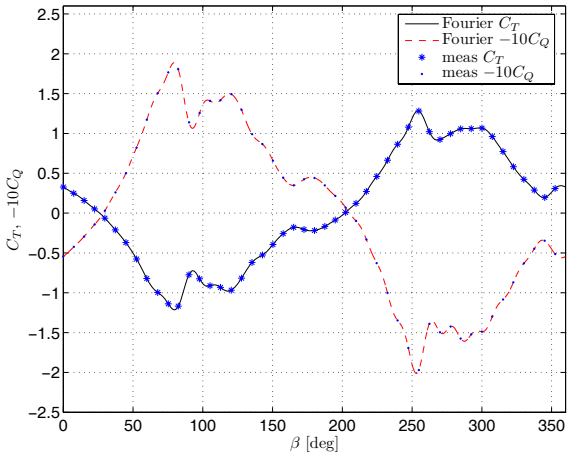

Figure 7: Propeller four-quadrant open-water characteristics.

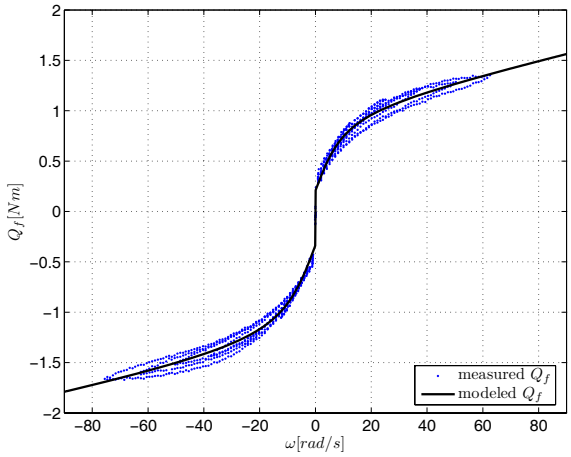

Figure 8: Friction torque: computed from measurements and a static approximation.

Some tests were performed with different profiles of towing carriage speed and various types of motor torque: square, sinusoidal and triangular waves of different amplitudes and frequencies. This was done using the built-in torque controller of the motor driver. Other tests have been performed using the built-in velocity controller enabling control of the propeller shaft speed. To perform tests in rough sea conditions, regular waves of 0.2 m amplitude have been generated with the wave maker. At the same time the propeller was moving in a sinusoidal vertical motion to simulate the vertical oscillation that occurs in rough sea due to vessel motion and waves.

4.2 Friction Torque

The friction torque has been modeled as the static function of (2). Figure 8 shows the friction torque computed from measurements and the model which has been used in the observer. For the propeller tested, the losses due to the friction torque are quite high compare to a full scale propeller, where losses are usually less than 6%.

4.3 Results

The thrust estimation scheme has been validated with the observer gains L_1 and L_2 reported in Table 1.

Figure 9 shows results from a test where the carriage speed varies from 1 m/s to -1 m/s while the shaft speed assumes positive and negative values. Both the estimated thrust $\hat{T}_p$ and torque $\hat{Q}_p$ are very accurate. In Figure 9, the thrust computed through (22), (23) and (25) with the four-quadrant characteristic C_T depicted in Figure 7 is reported. In (25) the speed of the towing carriage u has been used instead of the unknown advance speed u_a. When the carriage speed is positive the computed thrust is lower than the measured one because, due to the metallic grid, the advance speed is lower than the carriage speed. When the carriage speed is negative, the thrust computed with the propeller characteristic is about the average of the measured thrust because the advance speed is equal to vessel speed. When the vessel travels backwards the inlet water flow is not affected by the grid which is placed upstream of the propeller.

Figure 10 shows the result of a test performed in regular waves with height 0.20 m and the propeller moved along its vertical axis with a sinusoidal motion. Figure 10 (c) shows the vertical displacement along the propeller vertical axis that points upwards as shown in Figure 6. The propeller shaft speed has been kept constant at 38rad/s. A drop of thrust and torque occurs when the propeller rotates close to the water surface since the load decreases due to ventilation. The oscillations of torque, due to waves that disturb the inflow to the propeller, are well reproduced by the estimate. The estimated thrust is not as accurate as for the test without waves but the drop is properly captured and the estimation error is small. The results show that even in this extreme case, the estimates provided are quite accurate.

5 Conclusion

In this paper, a thrust estimation scheme for marine propellers was experimentally tested in waves to reproduce rough sea conditions and with a device that simulates the presence of a vessel hull. The scheme in-

Table 1: Observer parameters

Parameter	Value	Parameter	Value
$J_m[Kgm^2]$	$5.84 \cdot 10^{-3}$	ϵ	$1 \cdot 10^{-6}$
k_{f1}	$1.8 \cdot 10^{-2}$	τ_Q $[s]$	10
k_{f_2}	$1.29 \cdot 10^{-2}$	L_1	3.5
k_{f_3}	$6.96 \cdot 10^{-1}$	L_2	$-1/J_m$
k_{f_4}	$8.03 \cdot 10^{-1}$		

cluded a nonlinear observer to estimate the propeller torque and a mapping to compute the thrust from the observed torque. The advance speed was assumed to be unknown and only measurements of shaft speed and motor torque were used. Good Experimental results showed good performance in terms of accuracy of the thrust estimate.

6 Acknowledgment

The authors acknowledge Professor Sverre Steen for valuable suggestions and discussions. The Norwegian Research Council is acknowledged as the main sponsor of this project.

References

Bachmayer, R., Whitcomb, L. L., and Grosenbaugh, M. A. An accurate four-quadrant nonlinear dynamical model for marine thrusters: Theory and experimental validation. *IEEE Journal of Oceanic Engineering*, 2000. 25(1):146–159.

Blanke, M., Lindegaard, K., and Fossen, T. I. Dynamic model for thrust generation of marine propellers. In *5th IFAC Conference of Manoeuvring and Control of Marine craft (MCMC)*. Aalborg, Denmark, 2000 pages 363–368.

Guibert, C., Foulon, E., Aït-Ahmed, N., and Loron, L. Thrust control of electric marine thrusters. In *31nd Annual Conference of IEEE Industrial Electronics Society. IECON 2005*. Raleigh, North Carolina, USA, 2005 .

Khalil, H. K. *Nonlinear Systems*. Prentice Hall, third edition, 2000.

Pivano, L., Fossen, T. I., and Johansen, T. A. Nonlinear model identification of a marine propeller over four-quadrant operations. In *14th IFAC Symposium on System Identification, SYSID*. Newcastle, Australia, 2006a .

Pivano, L., Smogeli, Ø. N., Johansen, T. A., and Fossen, T. I. Marine propeller thrust estimation in four-quadrant operations. In *45th IEEE Conference on Decision and Control*. San Diego, CA, USA, 2006b .

Smogeli, Ø. N. *Control of Marine Propellers: From Normal to Extreme Conditions*. Ph.D. thesis, Department of Marine Technology, Norwegian University of Science and Technology (NTNU), Trondheim, Norway, 2006.

Smogeli, Ø. N., Ruth, E., and Sorensen, A. J. Experimental validation of power and torque thruster control. In *IEEE 13th Mediterranean Conference on Control and Automation (MED'05)*. Cyprus, 2005 pages 1506– 1511.

Van Lammeren, W. P. A., Manen, J. D. V., and Oosterveld, M. W. C. The Wageningen B-Screw Series. *Transactions of SNAME*, 1969.

Whitcomb, L. L. and Yoerger, D. Developement, comparison, and preliminary experimental validation of nonlinear dynamic thruster models. *IEEE Journal of Oceanic Engineering*, 1999. 24(4):481–494.

Zhinkin, V. B. Determination of the screw propeller thrust when the torque or shaft power is known. In *Fourth international symposium on practical design of ships and mobile units*. Bulgaria, 1989 .

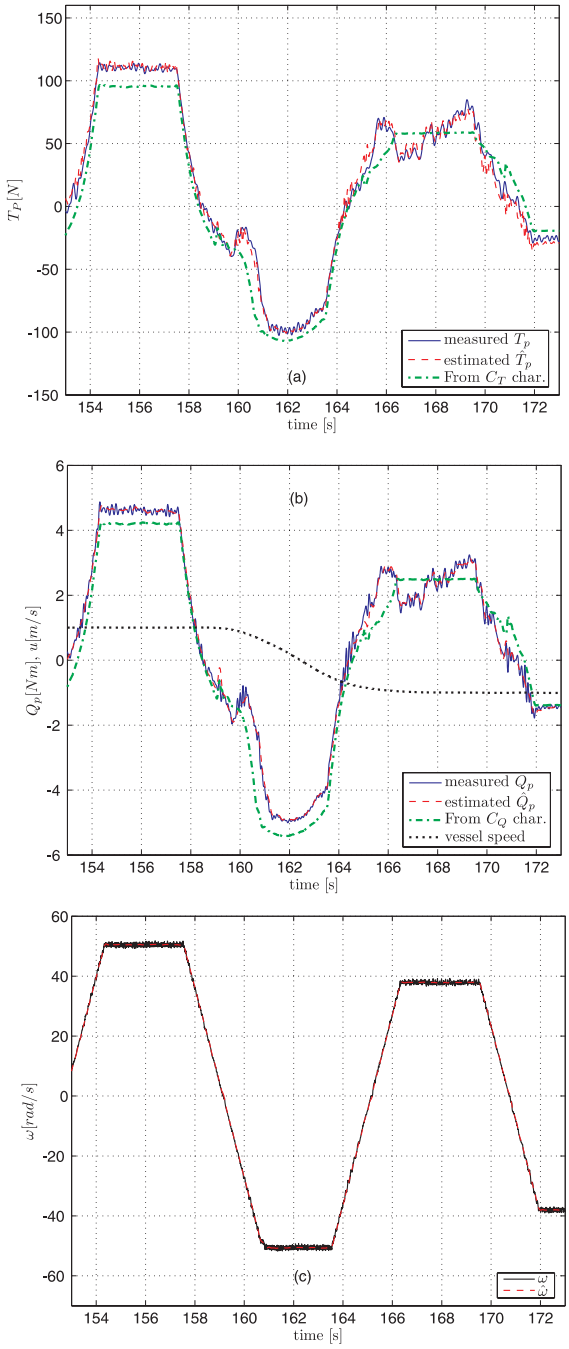

Figure 9: Experimental results with the vessel in motion.

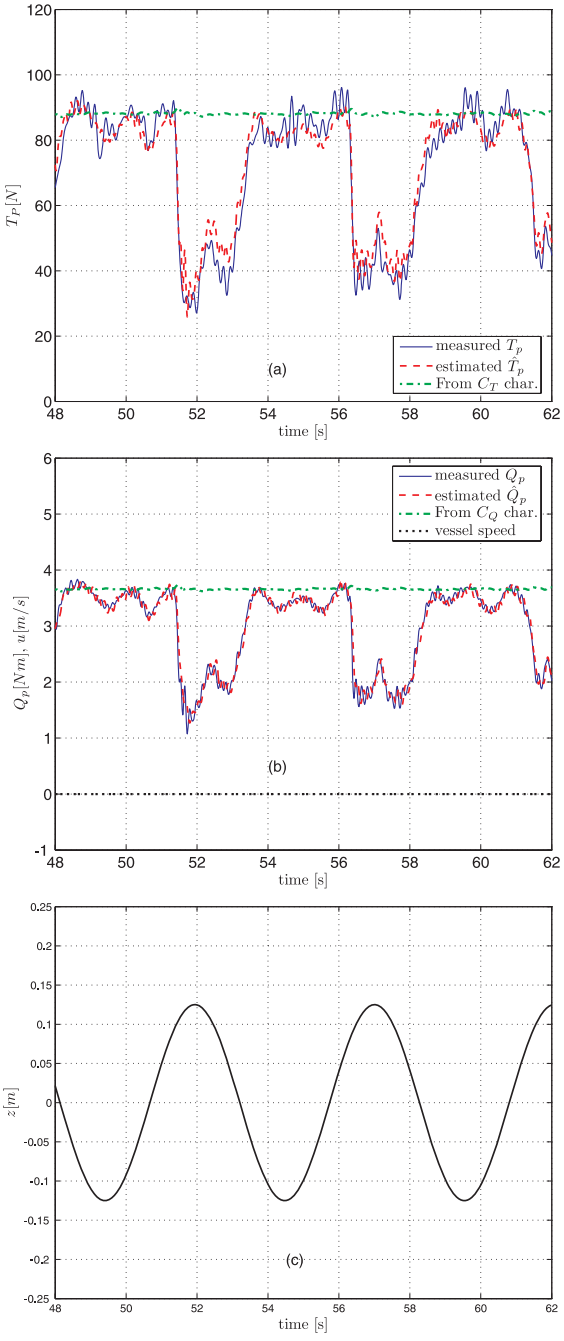

Figure 10: Experimental results with waves and constant shaft speed.